




Unraveling the sign reversal of the anomalous Hall effect in ferromagnet/heavy-metal ultrathin films

Yao Zhang ^{1,2} David Cortie,^{3,4} Thomas LaGrange,⁵ Waitung Lee,⁴ Tane Butler ¹,
Bart Ludbrook ¹ and Simon Granville^{1,2,*}

¹Robinson Research Institute, Victoria University of Wellington, Wellington 6140, New Zealand

²MacDiarmid Institute for Advanced Materials and Nanotechnology, Wellington 6011, New Zealand

³Institute for Superconducting and Electronic Materials, University of Wollongong, Wollongong, NSW 2500, Australia

⁴The Australian Nuclear Science and Technology Organisation, Lucas Heights, NSW 2232, Australia

⁵Laboratory of Ultrafast Microscopy and Electron Scattering, École Polytechnique Fédérale de Lausanne EPFL, Lausanne 1015, Switzerland



(Received 12 January 2023; accepted 28 February 2023; published 10 March 2023)

The sign reversal in the anomalous Hall effect (AHE) that occurs for material offers great prospects for AHE-based spintronic devices design. However, the mechanisms are still controversial in ultrathin ferromagnetic/heavy metal thin film systems due to the complicatedly interfacial effects. Here, we investigate the AHE sign reversal in ultrathin ferromagnetic $\text{Mn}_2\text{CoAl/Pd}$ films, a system which has shown unusual AHE, significant spin-orbit coupling, and magnetic texturing. Element-sensitive cross-sectional STEM imaging and the depth-resolved magnetization profile from polarized neutron reflectometry identifies the presence of a second ferromagnetic layer from intermixed Co-Pd. To quantitatively explain the sign reversal of the AHE, we build a model based on two contributions, ferromagnetic Mn_2CoAl and the intermixed CoPd layer. We also clarify that contributions to the AHE from magnetic proximity and spin Hall effect are negligible. Our work demonstrates that interfacial alloying can be a critical factor and provides insightful methods to determine the origins of the AHE in ferromagnet/heavy-metal thin film systems.

DOI: [10.1103/PhysRevB.107.094408](https://doi.org/10.1103/PhysRevB.107.094408)

I. INTRODUCTION

The anomalous Hall effect (AHE) is a phenomenon in which a large transverse resistivity can be observed in ferromagnetic materials due to the spin-orbit interaction. It is well known that AHE originates from the intrinsic mechanism related to the Berry curvature and extrinsic mechanisms including the side jump and skew scattering [1]. This effect shows potential applications for magnetic field sensing [2], spin-transfer torque [3], and spin-orbit torque generation [4].

The sign of AHE depends on the material and temperature of a single magnetic layer of the thin films. Generally, there are two mechanisms. In the case of the AHE from intrinsic Berry curvature, the sign of AHE can be tuned by doping due to the Fermi level shifting [5–7]. Another situation is where there are two magnetic sublattices in a material, usually rare-earth–transition-metal alloy, and the total AHE is a sum of contributions from the sublattices [8,9]. Because of the antiparallel alignments and different temperature dependences of the magnetic behavior of the two sublattices [5,10], a sign crossover can be seen in the temperature dependence of the total AHE.

However, in ferromagnet/heavy-metal ultrathin film systems, the mechanisms of the AHE sign reversal are still controversial because there are extra contributions from the

surface and interface where rich spin-dependent phenomena, such as the spin Hall effect and magnetic proximity effect appear due to the spin-orbit coupling and symmetry breaking [11]. For instance, Rosenblatt *et al.* [12] and Guo *et al.* [13], reported that the dominance of the surface scattering, having the AHE polarity opposite to that of bulk leads to the reversal of the AHE sign in Co/Pd multilayer. Different groups have proposed that the magnetized interfacial Pd, which arises due to the magnetic proximity effect, plays a more critical role than the surface scattering [14,15]. Very recently, Dang *et al.*, reported that the magnetic proximity effect cannot explain the sign reversal and concluded that the nonlocal spin conductivity induced by a spin-polarized current from the ferromagnetic layer injected into the nonmagnetic layer is the reason [16]. Thus, it is highly desirable to directly characterize the interfacial structure and magnetization together, which may disentangle these mechanisms.

To clarify and unravel the origins of the sign reversal of AHE in ferromagnet/heavy-metal ultrathin film systems, we chose a simple trilayer system, $\text{MgO/Mn}_2\text{CoAl/Pd}$ thin film, where we only need to consider one magnetically active interface, between the Mn_2CoAl and Pd layer. The inverse Heusler ferromagnetic compound Mn_2CoAl is a spin-gapless semiconductor exhibiting a band gap in one of the spin channels and a zero-band gap in the other [17,18], which bridges the gap between semiconductors and half-metallic ferromagnets, having a 100% spin polarization and showing great potential for spintronics applications. Perpendicular

*simon.granville@vuw.ac.nz

magnetic anisotropy (PMA) and skyrmions, a nanoscale type of topological spin texture, have been observed in MgO/Mn₂CoAl/Pd thin films due to the strong spin-orbit coupling and Dzyaloshinskii-Moriya interaction at the interface between the Pd and Mn₂CoAl layer [19–21], which make this material more attractive for ultralow-power and ultrahigh-density devices [22,23].

In this work, we investigated the sign change of AHE that occurs in MgO/Mn₂CoAl/Pd trilayers when changing the thickness of the Pd layer. By directly measuring the element-sensitive of the cross-sectional STEM structure and its depth-resolved magnetization profile with polarized neutron reflectometry, we demonstrated that the sign change of AHE results from the opposite sign of the AHE in the Mn₂CoAl layer and the intermixed CoPd alloy. A model based on these two contributions quantitatively that explains the sign change of AHE is presented.

II. EXPERIMENTAL METHOD

Two series of trilayers, series A: MgO(1.6 nm)/Mn₂CoAl(2.6 nm)/Pd(2.2–4.0 nm) and series B: MgO(1.6 nm)/Mn₂CoAl(3.7 nm)/Pd(0.86–8.64 nm), were deposited on thermally oxidized Si/SiO₂(300 nm) substrates by magnetron sputtering with a base pressure below 4×10^{-8} Torr. Samples were grown at ambient temperature using an Ar plasma while rotating the sample holder and then postgrowth annealed *in situ* for 1 h at 300 °C. The x-ray reflectivity has calibrated the growth rate of each layer.

Magneto-optical Kerr effect (MOKE) measurements with a green light ($\lambda = 540$ nm) were used to obtain the hysteresis loops at ambient temperature, using a MOKE microscope (MagVision, Vertis). In addition, the anomalous Hall resistance was measured at 300 K by using the resistivity option of a Physical Property Measurement System (PPMS, Quantum Design).

High-resolution scanning transmission electron microscopy (HRSTEM) and energy dispersive spectroscopy (EDS) investigations were conducted in Thermo Fisher Scientific (TFS) Titan Themis operating at 300 kV. Electron transparent, cross-sectional TEM films were prepared by tripod mechanical polishing. No ion milling was used to avoid artifacts arising from redeposition, ion mixing, and heating. Quantitative analysis and normalized line scan plots were processed using the TFS VELOX software program.

Polarized neutron reflectometry was conducted using the PLATYPUS reflectometer at the Australian Nuclear Science and Technology Organisation (ANSTO). More details have been shown in the Supplemental Material [24].

III. RESULTS

A. Pd thickness dependence of magnetic properties

In ferromagnet/heavy-metal ultrathin film systems, PMA relates to the nonmagnetic heavy-metal layer due to the spin-orbit interaction [25,26]. Here, we prepared Series A: MgO(1.6 nm)/Mn₂CoAl(2.6 nm)/Pd(2.2–4.0 nm) by modifying the thickness of Pd (t_{Pd}) to adjust the magnetic properties in Mn₂CoAl trilayers. The thicknesses of Mn₂CoAl and Pd

have been chosen from a range known to cover the change from in-plane to PMA [27].

Figure 1(a) shows the t_{Pd} dependence of out-of-plane (OP) hysteresis loops for the trilayers measured by a magneto-optical Kerr effect (MOKE) setup at ambient temperature. Square loops can be observed for trilayers with $t_{\text{Pd}} = 2.2$ –3.6 nm, confirming PMA. However, once t_{Pd} increases above 3.6 nm, the loops are in the spin-reorientation transition where the magnetic easy axis rotates from OP to the in-plane (IP) direction. Figures 1(b)–1(d) show the t_{Pd} -dependent crucial parameters: remanent ratio (M_r/M_s), coercive field ($\mu_0 H_c$), and effective magnetic anisotropy (K_{eff}), where M_r is the remanent magnetization and M_s is the saturation magnetization, taken as 315 emu/cm^3 [28]. In Fig. 1(b), the value of M_r/M_s equals 1 for trilayers $t_{\text{Pd}} = 2.2$ –3.6 nm indicating that the remanent magnetization keeps the same direction as that of the saturation magnetization, namely OP direction, but it suddenly drops to close to 0 meaning that the magnetization starts toward to IP direction. $\mu_0 H_c$ decreases as increasing t_{Pd} , as shown in Fig. 1(c). K_{eff} is defined by $1/2\mu_0 H_k M_s$, where $\mu_0 H_k$ is the anisotropy field, which can be fitted by the Stoner-Wohlfarth model as shown in our previous work [28]. The anisotropy field ($\mu_0 H_k$) shows variation that depends on t_{Pd} , similar to the variations observed for the coercive field ($\mu_0 H_c$). This indicates that the PMA of thin films of Mn₂CoAl becomes weaker as the thickness of the films increase.

B. Sign reversal of AHE

After understanding the magnetic properties of Mn₂CoAl trilayers with different Pd thicknesses, we systematically study the AHE for series B: MgO(1.6 nm)/Mn₂CoAl(3.7 nm)/Pd(0.86–8.64 nm) trilayers at 300 K as shown in Fig. 2. In the regime where t_{Pd} is small [see Fig. 2(a)], an AHE curve with a positive anomalous Hall resistance, $R_{\text{AHE}} = 0.83 \text{ } \Omega$, is observed at 0.86 nm Pd. By increasing t_{Pd} , R_{AHE} decreases and then disappears at 1.73 nm Pd. By continuing to increase t_{Pd} from 1.73–5.18 nm, square hysteresis loops can be obtained. More interestingly, a sign change of the AHE from positive to negative is observed in Figs. 2(b) and 2(c). After reaching a maximum, R_{AHE} decreases again and tends toward to zero with a thick Pd layer. The coercive field obtained from the AHE decreases with thicker Pd layer which is in line with the result of the MOKE measurements for series A [see Fig. 1(b)]. Furthermore, the remanent of the anomalous Hall effect is close to 0 for the sample with $t_{\text{Pd}} = 5.18$ nm in series B, as shown in Fig. 2(c), which strongly suggests that the PMA is weak with a thicker Pd layer. After subtracting the ordinary Hall effect, the saturation R_{AHE} is extracted and plotted as a function of t_{Pd} , as shown in Fig. 3.

Overall, by increasing t_{Pd} , R_{AHE} decreases from positive to negative with a maximum value at 3.46 nm, and finally decays to zero. In our recent work [27], we observed an unusual peak and sign reversal in AHE for these types of thin films. We hypothesized that there is an intermixed CoPd layer formed at the interface with an opposite sign of AHE as the Mn₂CoAl layer, which convincingly explains the thickness and temperature behaviors of this unusual peak. Here, we develop this hypothesis further to account for the sign change of the AHE.

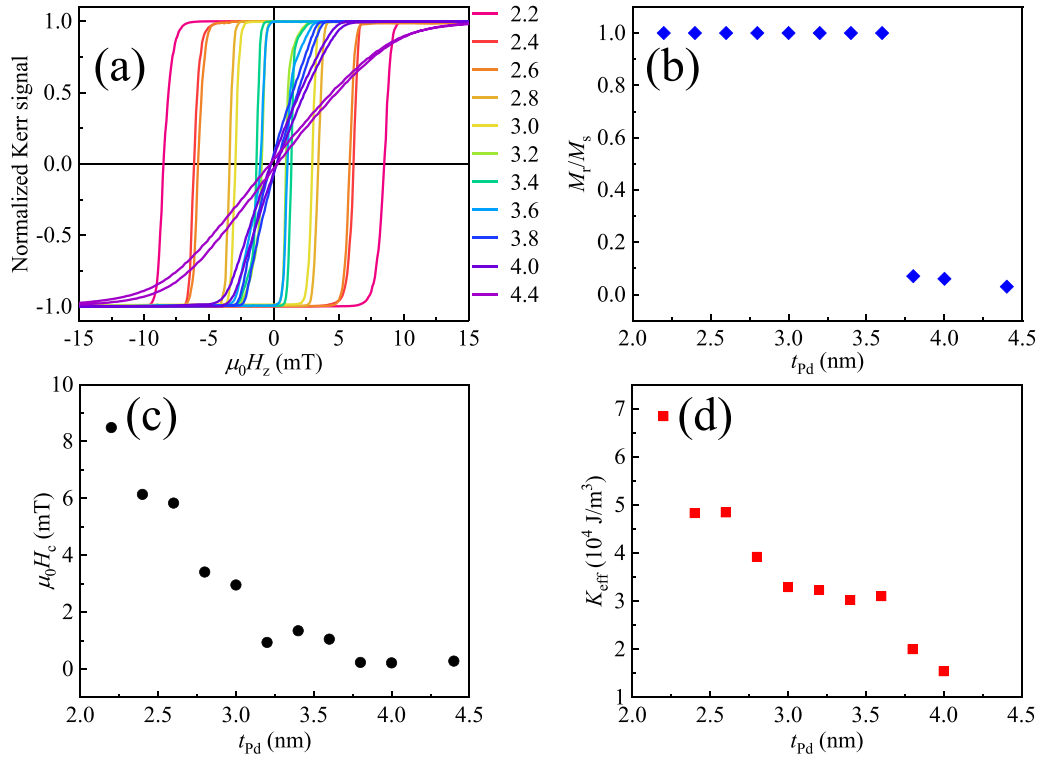


FIG. 1. (a) Magnetic hysteresis loops of series A: MgO(1.6 nm)/Mn₂CoAl(2.6 nm)/Pd(2.2–4.4 nm) trilayers measured under an OP magnetic field at ambient temperature. (b)–(d) Extracted M_f/M_s , $\mu_0 H_c$, and K_{eff} as a function of t_{Pd} .

C. Cross-sectional structure

To confirm this hypothesis, an intermixed CoPd alloy formed at the interface. We characterized the cross-sectional structure of the Mn₂CoAl trilayer by high-resolution scanning transmission electron microscopy (HRSTEM). Figure 4(a) shows the high-angle annular dark-field (HAADF) images and energy-dispersive x-ray spectroscopy (EDS) elemental maps. One can see that the elemental distribution of Co shows significant overlap with the top Pd layer indicating an intermixed CoPd alloy formed. Furthermore, the Mn and Al atoms have partially diffused into the bottom MgO layer. Figure 4(b) shows the normalized line profiles of the elemental maps across the trilayer. Notably, significant Al interdiffusion from Mn₂CoAl into MgO resulted in the formation of an Mg-Al-O insulating barrier. This interdiffusion can promote

the hybridization between Co and O orbitals at the interface, which plays an important role in PMA [29].

D. Depth-resolved magnetization profile

The previous section shows that an intermixed CoPd alloy is formed at the Mn₂CoAl/Pd interface, as well as Mn and Al atom diffusion into the MgO layer. To clarify the effect on the magnetism, depth-resolved magnetization profiling was performed by using polarized neutron reflectometry (PNR) measurements, which can track the magnetization at the sub-nm resolution as shown in Fig. 5. The reflectivity of R^{++} and R^{--} spin channels as a function of the scattering vector, Q_z , is displayed in Fig. 5(a), where R^{++} and R^{--} represent the spin-up and spin-down incoming neutrons. The measurement is performed at 10 K and 1 T field. The amplitude of the

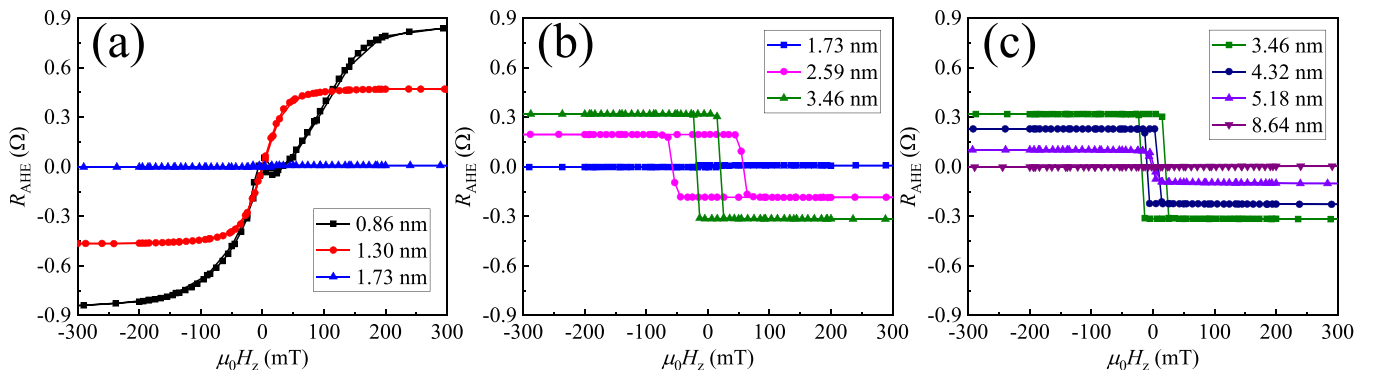


FIG. 2. Anomalous Hall effect for series B: MgO(1.6 nm)/Mn₂CoAl(3.7 nm)/Pd(0.86–8.64 nm) trilayers at 300 K.

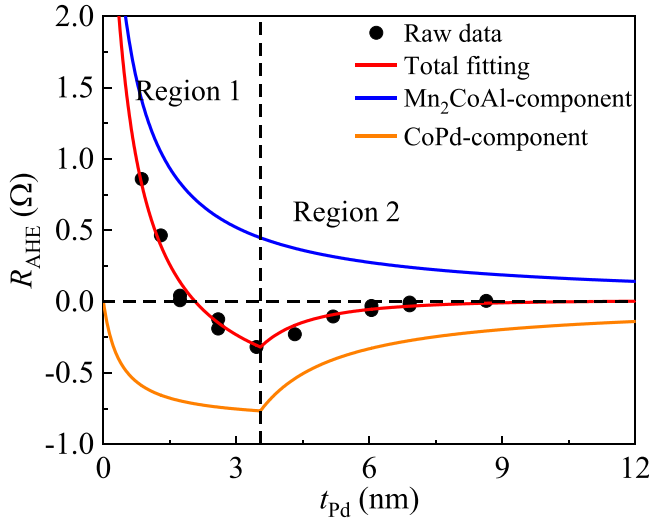


FIG. 3. The experimental R_{AHE} as a function of t_{Pd} with the fitting by a model based on the Mn_2CoAl and intermixed CoPd alloy. Both contributions are shown individually as well.

difference of the spin-dependent neutron reflectivity gives information on the magnetization depth profile, and is sensitive to the in-plane magnetization vector.

By fitting the PNR data, the nuclear, R^{++} and R^{--} depth scattering length density (SLD) profiles can be modeled [see Fig. 5(b)] so that the depth magnetization profile of the Mn_2CoAl trilayer can be resolved [see the orange curve of Fig. 5(b)]. A relatively thick magnetically dead layer of 1.5 nm was observed at the interface between the Mn_2CoAl layer and MgO substrate. By linking with the STEM results, we ascribe this dead layer to the Mn and Al atom diffusion from the Mn_2CoAl layer into the MgO layer. On the other hand, the calculated effective magnetization of the Mn_2CoAl layer (720 emu/cm^3) in the depth magnetization profile is higher than the Mn_2CoAl saturation magnetization obtained from the SQUID measurement (315 emu/cm^3). The reason is that the local composition of the Mn_2CoAl layer was lost with an Mn-Al-deficient and Co-rich structure, which increases the layers magnetization to that of bulk Co, which has a large magnetization, 1440 emu/cm^3 [30]. As the Mn has a negative neutron scattering length, and the cobalt, Al have a positive neutron scattering length, the neutron reflectometry is very sensitive to the ratio of Mn to the other elements. A fully stoichiometric Mn_2CoAl layer (mass density = 6.5 g/cm^3) should have a net neutron SLD of $-0.3 \times 10^{-6} \text{ \AA}^{-2}$, however, the films here have a value of $-0.1 \times 10^{-6} \text{ \AA}^{-2}$, which is consistent a lower Mn ratio (nominally $\text{Mn}_{1.7}\text{CoAl}$). At the interface between the Mn_2CoAl and Pd layers, an intermixed CoPd region was observed by STEM. This corresponds to the region of sharply decreased magnetization of 223 emu/cm^3 , which finally decays to 0 over a range of 3 nm. The modeled magnetization of this region agrees with that of a Pd-rich CoPd alloy, which is usually less than 200 emu/cm^3 [31].

There may be an additional contribution to the magnetic properties of these stacks from the ordinarily nonmagnetic Pd. It is known that the density of states in nonmagnetic Pd at the Fermi energy nearly satisfies the Stoner criterion in which

ferromagnetism is expected to occur when $N(E_F)I > 1$, where N and I are the density of states at the Fermi energy and Stoner parameter, respectively [32]. Therefore, by contacting a ferromagnetic material, the first few layers of Pd can be magnetized due to the so-called magnetic proximity effect [33]. From the PNR results, the SLD of the top layer is $3.5 \times 10^{-6} \text{ \AA}^{-2}$, which is between the theoretical neutron SLD of Pd ($3.98 \times 10^{-6} \text{ \AA}^{-2}$) and $\text{Co}_{50}\text{Pd}_{50}$ ($3.2 \times 10^{-6} \text{ \AA}^{-2}$). The fitted SLD shows the Pd at the top of the film has the same value as that of normal nonmagnetized Pd. This shows that the magnetization from the top part of the stack is dominant by the intermixed CoPd alloy, and the magnetic proximity effect is minimal in this system.

E. Two-contribution model

Now, we build a model to understand and disentangle the mechanisms contributing to the thickness dependence of the AHE and the sign change. From the STEM images and the PNR depth magnetization profile, we believe AHE in our system is dominated by two contributions from the ferromagnetic Mn_2CoAl layer and the intermixed CoPd alloy. Thus, we build a two-contribution model based on the electric current flowing through three separately considered conducting layers (see Supplemental Material [24]): a ferromagnetic Mn_2CoAl layer, with a constant anomalous Hall resistance ($R_{\text{AHE}}^{\text{MCA}}$); a CoPd intermixing layer, with an anomalous Hall resistance ($R_{\text{AHE}}^{\text{CoPd}}$); and a nonmagnetic Pd layer, with zero magnetization and no RAHE. These three conducting layers can be modeled as three resistors in parallel.

There are two thickness regions of interest in this model, labeled in Fig. 3. For region 1, we suppose the whole, very thin, Pd layer intermixes with Co and forms a magnetic CoPd intermixing layer on the top of the stack. The measured total R_{AHE} of the trilayer in this region can be written as

$$R_{\text{AHE}} = R_{\text{AHE}}^{\text{MCA}} \left(\frac{\rho_{\text{CoPd}} t_{\text{MCA}}}{\rho_{\text{MCA}} t_{\text{CoPd}} + \rho_{\text{MCA}} t_{\text{CoPd}}} \right) + R_{\text{AHE}}^{\text{CoPd}} \left(\frac{\rho_{\text{MCA}} t_{\text{CoPd}}}{\rho_{\text{MCA}} t_{\text{CoPd}} + \rho_{\text{MCA}} t_{\text{CoPd}}} \right),$$

where ρ_{MCA} , ρ_{CoPd} , t_{MCA} , and t_{CoPd} are the resistivity of Mn_2CoAl , the resistivity of CoPd intermixing layer, the thickness of Mn_2CoAl , and the thickness of the CoPd intermixing layer, respectively. For region 2, with increasing thickness of Pd, we suppose the Co cannot penetrate entirely through the Pd. Hence the thickness of the CoPd intermixing layer reaches a maximum value, and the remaining thickness of the Pd layer remains unmixed. The total R_{AHE} in this region can be written as

$$R_{\text{AHE}} = R_{\text{AHE}}^{\text{MCA}} \left(\frac{\rho_{\text{CoPd}} t_{\text{MCA}}}{\rho_{\text{MCA}} t_{\text{CoPd}} + \rho_{\text{MCA}} t_{\text{CoPd}}} \right) \times R_{\text{AHE}}^{\text{CoPd}} \left(\frac{\rho_{\text{MCA}} t_{\text{CoPd}}}{\rho_{\text{MCA}} t_{\text{CoPd}} + \rho_{\text{MCA}} t_{\text{CoPd}}} \right) \times \left(\frac{\rho_{\text{Pd}} t_{\text{CoPd}}}{\rho_{\text{CoPd}} (t_{\text{Pd}} - t_{\text{CoPd}}) + \rho_{\text{Pd}} t_{\text{CoPd}}} \right),$$

where ρ_{Pd} is the resistivity of Pd. Note that the first term is the same as in region 1, and the second term is scaled

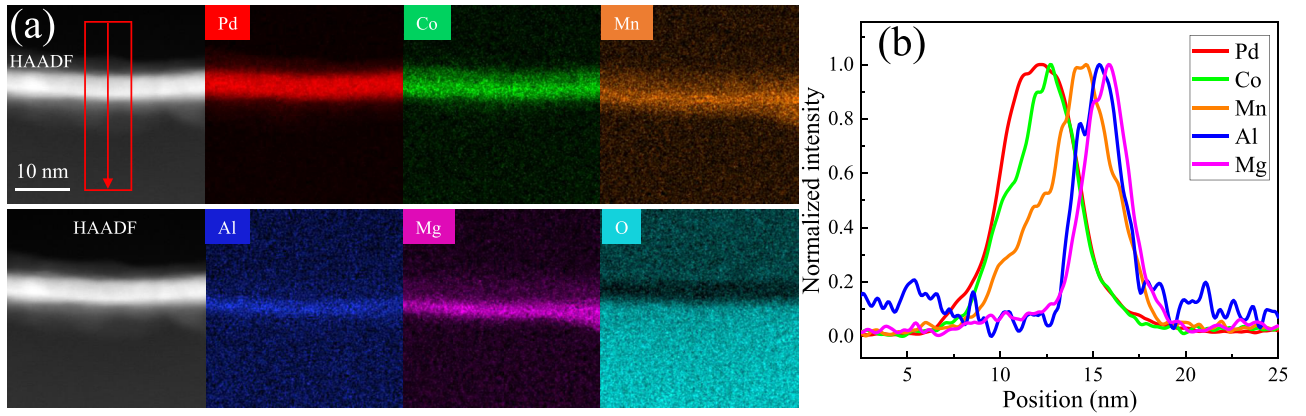


FIG. 4. (a) The cross-sectional high-resolution STEM images and EDS elemental maps for the Mn_2CoAl trilayer. (b) The normalized line profiles of the elemental maps across the trilayers. The line profile integrates a 5 nm width across the film [see the inset box and arrow in (a)].

by the fraction of the current that passes instead through the nonmagnetic Pd, and does not contribute to the total anomalous Hall resistance. $\rho_{\text{MCA}} = 219.5 \mu\Omega \text{ cm}$ and $\rho_{\text{Pd}} = 11.1 \mu\Omega \text{ cm}$ were obtained by fitting the thickness-dependent resistances of the trilayer with the Fuchs-Sondheimer model in the Supplemental Material [24] (see also, Refs. [34–38] therein). As the intermixed CoPd alloy is Pd rich, the resistance of the Pd and CoPd intermixing layer is supposed to be close. t_{MCA} is fixed at 2.2 nm after subtracting the dead layer detected by the PNR. The total fitting result has been presented as the red curve of Fig. 3, which gives an excellent agreement with the data. The maximum thickness of the CoPd intermixing layer is 3.5 nm obtained from the fitting, which is very close to the calculated value from the PNR results.

Both fitting components have been presented individually as well. The ferromagnetic Mn_2CoAl layer shows a positive AHE, which is in line with our previous work on thick, single-layer films [36]. With increasing t_{Pd} , the magnitude of $R_{\text{AHE}}^{\text{MCA}}$ decreases (see the blue curve of Fig. 3). The reason is that an increasing amount of the electric current passes through the CoPd and Pd layer as the resistivity of them is much lower than that of Mn_2CoAl , which is the so-called shunting effect. On the other hand, the intermixed CoPd alloy shows

a negative AHE, known for the CoPd alloy with excess Pd [39]. Regarding the Pd thickness dependence of $R_{\text{AHE}}^{\text{CoPd}}$, the magnitude increases first due to more CoPd formed. Once the maximum thickness of the CoPd region is reached at $t_{\text{Pd}} = 3.5 \text{ nm}$, the extra thickness of Pd is unmixed and induces a shunting effect through nonmagnetic Pd.

IV. DISCUSSION

Generally, the PMA is robust with a thicker heavy-metal layer [40]. However, the magnetic anisotropy is changed from out-of-plane to in-plane direction with a thicker Pd layer in our system. We should mention that our system with two PMA components is different from the conventional single PMA component. The origin of both PMA components is the spin-orbit coupling of the Co and Pd atoms, though the hybridization between the ferromagnetic atom Co and the oxygen atoms in MgO is another source. When the Pd layer is thicker, the effective thickness of Mn_2CoAl decreases while the thickness of intermixed CoPd layer increases. Thus, the Mn_2CoAl layer is not coupled to the Pd layer anymore, but coupled to CoPd alloy, which results in the disappear of PMA in Mn_2CoAl . For ultrathin ferromagnetic thin films, it

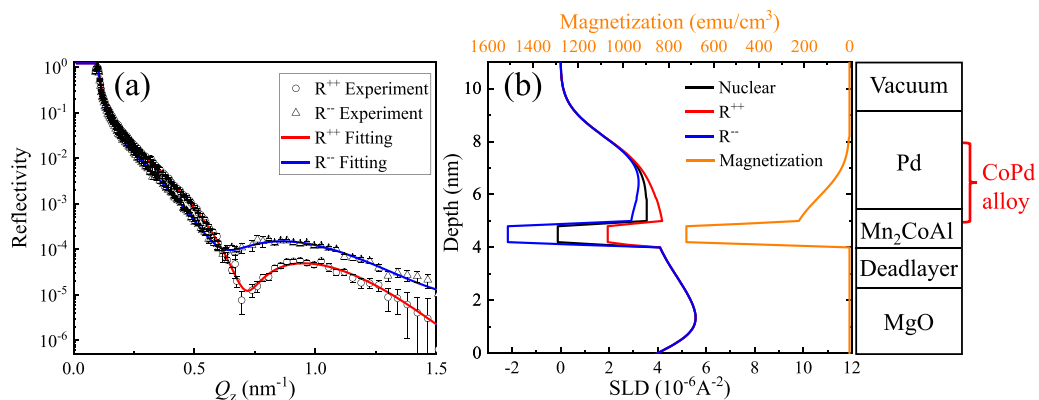


FIG. 5. (a) The experimental polarized neutron reflectivity and the fitted curves as a function of the scattering vector for Mn_2CoAl trilayer performed at 10 K under a 1 T external magnetic field. (b) The nuclear (black), R^{++} (red), and R^{--} (blue) scattering length density and saturation magnetization (orange) depth profiles.

is known that the PMA can be only observed in a very thin thickness [41,42]. With a thicker Pd layer, more CoPd alloy forms so that the thickness of CoPd alloy could be too thick to exhibit PMA.

Recently, the spin Hall magnetoresistance (SMR) effect has been observed in ferromagnet/heavy-metal thin film systems, with a similar thickness dependence to that of our AHE results in Fig. 3 [43–45]. In this effect, a spin current generated from the heavy-metal layer diffuses into the ferromagnet and thus changes the resistance of the ferromagnet. During this process, a spin current can be reflected from the ferromagnet into heavy metal and gives rise to an AHE-like transverse resistance, which is the so-called spin Hall-AHE [46,47]. This AHE resistance relates to t_{Pd} and can be written as

$$\frac{2\lambda_s^2\theta_{\text{SH}}^2}{t_{\text{Pd}}^2} \frac{G_i \tanh^2\left(\frac{t_{\text{Pd}}}{\lambda_s}\right)}{(\sigma_{\text{Pd}} + 2\lambda_s G_r \coth\frac{t_{\text{Pd}}}{\lambda_s})^2}$$

[46], where λ_s , θ_{SH} , G_i , G_r , and σ_{Pd} are the spin diffusion length, spin Hall angle, the imaginary part of spin-mixing conductance, the real part of spin-mixing conductance, and the conductivity of the Pd layer, respectively. We have fitted our data using a term from the spin Hall-AHE in the Supplemental Material [24] (see, also, Refs. [48–50] therein) and although the fitting looks acceptable, it requires an extremely high value of G_i , $\sim 10^{34} \Omega^{-1} \text{cm}^{-2}$, which is significantly greater than the value obtained in other systems, typically less than $10^{15} \Omega^{-1} \text{cm}^{-2}$ [43,47]. We also notice that spin Hall-AHE is usually very small, $\sim \text{m}\Omega$ [51,52], which is a

factor of 100 times smaller than the total R_{AHE} in our system. Therefore, we think the sign reversal of AHE in our stack cannot be explained by the spin Hall-AHE mechanism.

V. CONCLUSION

In summary, we prepared the MgO/Mn₂CoAl/Pd trilayers with various thicknesses of the Pd layer to explore the sign reversal of AHE. We first investigated the magnetic properties and AHE where a sign reversal of AHE from positive to negative was observed by increasing t_{Pd} . Then, using a combination of elemental-sensitive STEM and depth-resolved magnetization from PNR, we demonstrated an intermixed CoPd alloy formed at the interface. We ascribed the sign change of AHE to the opposite sign of AHE in the Mn₂CoAl layer and the intermixed CoPd alloy. A model based on these two contributions was built to unravel how the polarity of the AHE occurs with increasing Pd thickness. Our work demonstrates that interface-sensitive and depth-profiling techniques are essential for quantitatively disentangling the mechanisms behind unusual phenomena in the AHE and are necessary to check for possible contributions from the magnetic proximity effect and spin Hall-AHE.

ACKNOWLEDGMENT

The MacDiarmid Institute is supported under the New Zealand Centres of Research Excellence Programme.

-
- [1] N. Nagaosa, J. Sinova, S. Onoda, A. H. MacDonald, and N. P. Ong, Anomalous Hall effect, *Rev. Mod. Phys.* **82**, 1539 (2010).
- [2] Y. Lu, J. Cai, H. Pan, and L. Sun, Ultrasensitive anomalous Hall effect in SiO₂/FePt/SiO₂ sandwich structure films, *Appl. Phys. Lett.* **100**, 022404 (2012).
- [3] S. Iihama, T. Taniguchi, K. Yakushiji, A. Fukushima, Y. Shiota, S. Tsunegi, R. Hiramatsu, S. Yuasa, Y. Suzuki, and H. Kubota, Spin-transfer torque induced by the spin anomalous Hall effect, *Nature Electronics* **1**, 120 (2018).
- [4] T. Y. Ma, C. H. Wan, X. Wang, W. L. Yang, C. Y. Guo, C. Fang, M. K. Zhao, J. Dong, Y. Zhang, and X. Han, Evidence of magnetization switching by anomalous spin Hall torque in NiFe, *Phys. Rev. B* **101**, 134417 (2020).
- [5] Z. Fang, N. Nagaosa, K. S. Takahashi, A. Asamitsu, R. Mathieu, T. Ogasawara, H. Yamada, M. Kawasaki, Y. Tokura, and K. Terakura, The anomalous Hall effect and magnetic monopoles in momentum space, *Science* **302**, 92 (2003).
- [6] W.-L. Lee, S. Watauchi, V. Miller, R. Cava, and N. Ong, Dissipationless anomalous Hall current in the ferromagnetic spinel CuCr₂Se_{4-x}Br_x, *Science* **303**, 1647 (2004).
- [7] K. S. Takahashi, M. Onoda, M. Kawasaki, N. Nagaosa, and Y. Tokura, Control of the Anomalous Hall Effect by Doping in Eu_{1-x}La_xTiO₃ Thin Films, *Phys. Rev. Lett.* **103**, 057204 (2009).
- [8] Y. Mimura, N. Imamura, and Y. Koshiro, Hall effect in rare-earth-transition-metal amorphous alloy films, *J. Appl. Phys.* **47**, 3371 (1976).
- [9] R. Asomoza, I. Campbell, H. Jouve, and R. Meyer, Extraordinary Hall effect in rare-earth-cobalt amorphous films, *J. Appl. Phys.* **48**, 3829 (1977).
- [10] O. S. Anilturk and A. R. Koymen, Element-specific magnetization of a Gd-Co composite system using spin-polarized Auger electron spectroscopy, *Phys. Rev. B* **68**, 024430 (2003).
- [11] F. Hellman, A. Hoffmann, Y. Tserkovnyak, G. S. D. Beach, E. E. Fullerton, C. Leighton, A. H. MacDonald, D. C. Ralph, D. A. Arena, H. A. Durr, P. Fischer, J. Grollier, J. P. Heremans, T. Jungwirth, A. V. Kimel, B. Koopmans, I. N. Krivorotov, S. J. May, A. K. Petford-Long, J. M. Rondinelli, N. Samarth, I. K. Schuller, A. N. Slavin, M. D. Stiles, O. Tchernyshyov, A. Thiaville, and B. L. Zink, Interface-induced phenomena in magnetism, *Rev. Mod. Phys.* **89**, 025006 (2017).
- [12] D. Rosenblatt, M. Karpovski, and A. Gerber, Reversal of the extraordinary Hall effect polarity in thin Co/Pd multilayers, *Appl. Phys. Lett.* **96**, 022512 (2010).
- [13] Z. B. Guo, W. B. Mi, R. O. Aboljadayel, B. Zhang, Q. Zhang, P. G. Barba, A. Manchon, and X. X. Zhang, Effects of surface and interface scattering on anomalous Hall effect in Co/Pd multilayers, *Phys. Rev. B* **86**, 104433 (2012).
- [14] V. Keskin, B. Aktaş, J. Schmalhorst, G. Reiss, H. Zhang, J. Weischenberg, and Y. Mokrousov, Temperature and Co thickness dependent sign change of the anomalous Hall effect in Co/Pd multilayers: An experimental and theoretical study, *Appl. Phys. Lett.* **102**, 022416 (2013).

- [15] H. Fu, C. You, L. Ma, N. Tian, F. Xin, Z. Cheng, A. Basha, and A. Kohn, Interfacial contributions to anomalous Hall effect in perpendicular magnetic anisotropic $[\text{Co}_2\text{MnSi}/\text{Pd}]_3$ multilayer, *Phys. Rev. Mater.* **2**, 124404 (2018).
- [16] T. H. Dang, Q. Barbedienne, D. Q. To, E. Rongione, N. Reyren, F. Godel, S. Collin, J. M. George, and H. Jaffrès, Anomalous Hall effect in $3d/5d$ multilayers mediated by interface scattering and nonlocal spin conductivity, *Phys. Rev. B* **102**, 144405 (2020).
- [17] S. Ouardi, G. H. Fecher, C. Felser, and J. Kübler, Realization of Spin Gapless Semiconductors: The Heusler Compound Mn_2CoAl , *Phys. Rev. Lett.* **110**, 100401 (2013).
- [18] X. Wang, Z. Cheng, G. Zhang, H. Yuan, H. Chen, and X.-L. Wang, Spin-gapless semiconductors for future spintronics and electronics, *Phys. Rep.* **888**, 1 (2020).
- [19] Y. Zhang, G. Dubuis, C. Doyle, T. Butler, and S. Granville, Nonvolatile and Volatile Skyrmion Generation Engineered by Ionic Liquid Gating in Ultrathin Films, *Phys. Rev. Appl.* **16**, 014030 (2021).
- [20] Y. Zhang, G. Dubuis, T. Butler, S. Kaltenberg, E. Trewick, and S. Granville, Voltage-Controlled Switching of Magnetic Anisotropy in Ambipolar $\text{Mn}_2\text{CoAl}/\text{Pd}$ Bilayers, *Phys. Rev. Appl.* **17**, 034006 (2022).
- [21] N. Sun, Y. Zhang, H. Fu, W. Che, C. You, and R. Shan, Perpendicular magnetic anisotropy in Mn_2CoAl thin film, *AIP Adv.* **6**, 015006 (2016).
- [22] B. Dieny and M. Chshiev, Perpendicular magnetic anisotropy at transition metal/oxide interfaces and applications, *Rev. Mod. Phys.* **89**, 025008 (2017).
- [23] X. Zhang, Y. Zhou, K. M. Song, T.-E. Park, J. Xia, M. Ezawa, X. Liu, W. Zhao, G. Zhao, and S. Woo, Skyrmion-electronics: writing, deleting, reading and processing magnetic skyrmions toward spintronic applications, *J. Phys.: Condens. Matter* **32**, 143001 (2020).
- [24] See Supplemental Material at <http://link.aps.org/supplemental/10.1103/PhysRevB.107.094408> for details of the PNR, two-contribution model, FS model, and alternative models.
- [25] J. Stöhr, Exploring the microscopic origin of magnetic anisotropies with x-ray magnetic circular dichroism (XMCD) spectroscopy, *J. Magn. Magn. Mater.* **200**, 470 (1999).
- [26] Y.-C. Lau, Z. Chi, T. Taniguchi, M. Kawaguchi, G. Shibata, N. Kawamura, M. Suzuki, S. Fukami, A. Fujimori, H. Ohno *et al.*, Giant perpendicular magnetic anisotropy in $\text{Ir}/\text{Co}/\text{Pt}$ multilayers, *Phys. Rev. Mater.* **3**, 104419 (2019).
- [27] Y. Zhang and S. Granville, Two-channel anomalous Hall effect originating from the intermixing in $\text{Mn}_2\text{CoAl}/\text{Pd}$ thin films, *Phys. Rev. B* **106**, 144414 (2022).
- [28] Y. Zhang, G. Dubuis, T. Butler, and S. Granville, Fractal Analysis of Skyrmions Generated by Field-Assisted Fine-tuning of Magnetic Anisotropy, *Phys. Rev. Appl.* **15**, 014020 (2021).
- [29] Z. Wen, J. P. Hadorn, J. Okabayashi, H. Sukegawa, T. Ohkubo, K. Inomata, S. Mitani, and K. Hono, Interdiffusion in epitaxial ultrathin $\text{Co}_2\text{FeAl}/\text{MgO}$ heterostructures with interface-induced perpendicular magnetic anisotropy, *Appl. Phys. Express* **10**, 013003 (2017).
- [30] J. M. Coey, *Magnetism and Magnetic Materials* (Cambridge University Press, Cambridge, 2010).
- [31] A. Bourezg and A. Kharmouche, Synthesis, structural and magnetic properties of $\text{Co}_{100-x}\text{Pd}_x/\text{GaAs}$ thin films, *Vacuum* **155**, 612 (2018).
- [32] E. C. Stoner, Collective electron ferromagnetism, *Proc. R. Soc. London A* **165**, 372 (1938).
- [33] P. Manna and S. Yusuf, Two interface effects: Exchange bias and magnetic proximity, *Phys. Rep.* **535**, 61 (2014).
- [34] D. Schumacher, New evidence for the validity of the Fuchs-Sondheimer theory, *Thin Solid Films* **152**, 499 (1987).
- [35] T. Zhou and D. Gall, Resistivity scaling due to electron surface scattering in thin metal layers, *Phys. Rev. B* **97**, 165406 (2018).
- [36] R. G. Buckley, T. Butler, C. Pot, N. M. Strickland, and S. Granville, Exploring disorder in the spin gapless semiconductor Mn_2CoAl , *Mater. Res. Exp.* **6**, 106113 (2019).
- [37] M. Angadi and S. Shivaprasad, Some transport properties of palladium films, *J. Mater. Sci.* **19**, 2396 (1984).
- [38] S. Shivaprasad, L. Udachan, and M. Angadi, Electrical resistivity of thin palladium films, *Phys. Lett. A* **78**, 187 (1980).
- [39] S. Das, G. Kopnov, and A. Gerber, Detection of hydrogen by the extraordinary Hall effect in CoPd alloys, *J. Appl. Phys.* **124**, 104502 (2018).
- [40] N.-H. Kim, D.-S. Han, J. Jung, K. Park, H. J. Swagten, J.-S. Kim, and C.-Y. You, Dependence of interfacial Dzyaloshinskii-Moriya interaction and perpendicular magnetic anisotropy on the thickness of the heavy-metal layer, *Appl. Phys. Exp.* **10**, 103003 (2017).
- [41] C. Fowley, N. Decorde, K. Oguz, K. Rode, H. Kurt, and J. Coey, Perpendicular magnetic anisotropy in CoFeB/Pd bilayers, *IEEE Trans. Magn.* **46**, 2116 (2010).
- [42] T. Liu, Y. Zhang, J. Cai, and H. Pan, Thermally robust $\text{Mo}/\text{CoFeB}/\text{MgO}$ trilayers with strong perpendicular magnetic anisotropy, *Sci. Rep.* **4**, 5895 (2014).
- [43] J. Kim, P. Sheng, S. Takahashi, S. Mitani, and M. Hayashi, Spin Hall Magnetoresistance in Metallic Bilayers, *Phys. Rev. Lett.* **116**, 097201 (2016).
- [44] M. Althammer, S. Meyer, H. Nakayama, M. Schreier, S. Altmannshofer, M. Weiler, H. Huebl, S. Geprägs, M. Opel, R. Gross *et al.*, Quantitative study of the spin Hall magnetoresistance in ferromagnetic insulator/normal metal hybrids, *Phys. Rev. B* **87**, 224401 (2013).
- [45] H. Nakayama, M. Althammer, Y. T. Chen, K. Uchida, Y. Kajiwara, D. Kikuchi, T. Ohtani, S. Geprägs, M. Opel, S. Takahashi, R. Gross, G. E. W. Bauer, S. T. B. Goennenwein, and E. Saitoh, Spin Hall Magnetoresistance Induced by a Nonequilibrium Proximity Effect, *Phys. Rev. Lett.* **110**, 206601 (2013).
- [46] Y.-T. Chen, S. Takahashi, H. Nakayama, M. Althammer, S. T. B. Goennenwein, E. Saitoh, and G. E. W. Bauer, Theory of spin Hall magnetoresistance, *Phys. Rev. B* **87**, 144411 (2013).
- [47] S. Meyer, R. Schlitz, S. Geprägs, M. Opel, H. Huebl, R. Gross, and S. T. Goennenwein, Anomalous Hall effect in YIG/Pt bilayers, *Appl. Phys. Lett.* **106**, 132402 (2015).
- [48] R. Ramos, T. Kikkawa, A. Anadón, I. Lucas, T. Niizeki, K. Uchida, P. A. Algarabel, L. Morellón, M. H. Aguirre, M. R. Ibarra *et al.*, Interface-induced anomalous Nernst effect in $\text{Fe}_3\text{O}_4/\text{Pt}$ -based heterostructures, *Appl. Phys. Lett.* **114**, 113902 (2019).
- [49] O. Inyang, L. Bouchenoire, B. Nicholson, M. Tokaç, R. M. Rowan-Robinson, C. J. Kinane, and A. T. Hindmarch, Threshold interface magnetization required to induce magnetic proximity effect, *Phys. Rev. B* **100**, 174418 (2019).
- [50] S. Mayr, J. Ye, J. Stahn, B. Knoblich, O. Klein, D. A. Gilbert, M. Albrecht, A. Paul, P. Böni, and W. Kreuzpaintner,

- Indications for Dzyaloshinskii-Moriya interaction at the Pd/Fe interface studied by in situ polarized neutron reflectometry, [Phys. Rev. B **101**, 024404 \(2020\)](#).
- [51] T. A. Peterson, A. P. McFadden, C. J. Palmstrøm, and P. A. Crowell, Influence of the magnetic proximity effect on spin-orbit torque efficiencies in ferromagnet/platinum bilayers, [Phys. Rev. B **97**, 020403\(R\) \(2018\)](#).
- [52] C. Guo, C. Wan, M. Zhao, H. Wu, C. Fang, Z. Yan, J. Feng, H. Liu, and X. Han, Spin-orbit torque switching in perpendicular $Y_3Fe_5O_{12}/Pt$ bilayer, [Appl. Phys. Lett. **114**, 192409 \(2019\)](#).